A New Hexagonal 16L Perovskite-Related Structure: $Ba_4Ca_{1-x}Mn_{3+x}O_{12-\delta}$

N. Floros, C. Michel,* M. Hervieu, and B. Raveau

Laboratoire CRISMAT, CNRS UMR 6508, ISMRA et Université de Caen, 6 Boulevard du Maréchal Juin, 14050 Caen Cedex, France

Received March 31, 2000. Revised Manuscript Received July 7, 2000

A new manganese oxide, $Ba_4Ca_{1-x}Mn_{3+x}O_{12-\delta}$, closely related to the hexagonal perovskite family has been synthesized. It crystallizes in the $P\bar{6}m2$ space group with $a = 5.8003(3)$ Å and $c = 38.958(1)$ Å. This structure derives from the rare hexagonal 16L polytype and exhibits ordered oxygen deficient vacancies, so that it can be described as the stacking along $\vec{c}$ of cubic (*c*) and hexagonal (*h*) [BaO_3] layers, with oxygen deficient cubic (*c*′) [BaO_2] layers, according to the sequence $(hhccc'cc)_2$. This framework forms octahedral layers occuped by manganese and calcium and tetrahedral layers occupied by manganese. These structural results, together with the chemical composition, confer to manganese an unusual mixed valency.

Introduction

One of the most fascinating structures in the area of solid-state chemistry is certainly the perovskite. The ability of its octahedral framework to accommodate various structural mechanisms (octahedra tilting, ion substitution and/or deficiency, crystallographic shearing, intergrowth, etc.) allows numerous new materials to be synthesized. Moreover, with combination of fundamental and applied relevance, each of these mechanisms is a way for generating or modifying physical properties. A huge number of works has been and is still devoted to the perovskite-related compounds. The famous superconducting cuprates[1] and colossal magnetoresistant manganites[2] have recently exemplified the potential of the perovskite-based oxides.

The description of the AMO_3 perovskite structure as a close packing of hexagonal AO_3 layers along $[111]_c$, with M cations located in octahedral sites, allows one to generate an unlimited number of polytypes closely related to the cubic perovskite. The latter is the result of the association of cubic (corner-sharing octahedra) and hexagonal (face-sharing octahedra) layers. The polytype structure is related to the ratio of cubic/hexagonal layers[3−5] which itself depends on numerous factors, such as the relative cation sizes, the anion and cation content, or the electronic configuration of the metallic elements. Moreover, even for a given compound, the thermal story is of importance, as recently shown for example by annealing $SrMnO_3$[6,7] or doping $BaMnO_3$.[8,9] This description allows one to shed light on another structural mechanism, namely a possible deficiency in M cations,[10,11] which is not common in the cubic perovskite, contrary to deficiencies in A cations and oxygen. The formulation of such M-deficient perovskites is $A_nM_{n-x}O_{3n}$.

Thus, many possibilities can be generated by controlling the aforementioned factors.[12−14] In this respect, the Ba−Ca−Mn−O system is very attractive, due to the fact that manganese is susceptible to introduce oxygen deficiency in hexagonal or cubic layers, as previously shown in $AMnO_{3-x}$ compounds,[15−17] where trigonal or square pyramidal MnO_5 polyhedra were observed. Moreover, alkaline earth cations are not always confined in 12-fold coordinated sites but may also sit in octahedral sites,[12,18−19] and various orderings between alkaline earth cations and manganese may also appear due to size differences.

In this paper, we report on a new manganese oxide, $Ba_4Ca_{1-x}Mn_{3+x}O_{12-\delta}$, with an original structure closely related to the rare hexagonal 16L perovskite and differing from the latter by an ordered oxygen deficiency, so that octahedral manganese and calcium layers

(1) Raveau, B.; Michel, C.; Hervieu, N.; Groult, D. *Crystal Chemistry of High T_c Superconducting Copper Oxides;* Springer-Verlag: Berlin, Heidelberg, 1991.
(2) *Colossal Magnetoresistance, Charge Ordering and Related Properties of Manganese Oxides*; Rao, C. N. R., Raveau, B., Eds.; World Scientific: Singapore, 1998.
(3) Negas, T.; Roth, R. S. *J. Solid State Chem*. **1970**, *3*, 323.
(4) Gushee, B. E.; Katz, L.; Ward, R. *Inorg. Chem*. **1957**, *79*, 5601.
(5) Potoff, A. D.; Chamberland, B. L. Katz, L. *J. Solid State Chem*. **1973**, *8*, 234.
(6) Negas, T.; Roth, R. S. *J. Solid State Chem*. **1970**, *1*, 409.
(7) Takeda, T.; Ohara, S. J. *J. Phys. Soc. Jpn*. **1974**, *37*, 275.
(8) Boullay, P.; Hervieu, M.; Labbe, P.; Raveau, B. *Mater. Res. Bull*. **1997**, *32*, 35.
(9) Donohue, P. C.; Katz, L.; Ward, R. *Inorg. Chem*, **1966**, *5*, 339
(10) Federov, N. F.; Mel'nikova, O. V.; Saltykova, V. A.; Chistyakova, M. V. *Russ. J. Inorg. Chem*. **1979**, *24*, 649.
(11) Schueckel, K.; Mueller-Buschbaum, H. *Z. Anorg. Allg. Chem*. **1985**, *523*, 69.
(12) Galasso, F. S. *Structure and Properties of Inorganic Compounds*; Pergamon Press: Oxford, U.K., 1970.
(13) Katz, L.; Ward, R. *Inorg. Chem*. **1964**, *3*, 205.
(14) Darriet, J.; Subramanian, M. A. *J. Mater. Chem*. **1995**, *5*, 543.
(15) Caignert, V.; Hervieu, M.; Domenges, B.; Nguyen, N.; Pannetier, J.; Raveau, B. *J. Solid State Chem*. **1998**, *73*, 107.
(16) Gonzalez-Calbet, J. M.; Parras, M.; Alonso, J. M.; Vallet-Regi, M. *J. Solid State Chem*. **1993**, *106*, 99.
(17) Jacobson, A. J.; Horrox, A. J. W. *Acta Crystallogr*. **1976**, *B32*, 1003.
(18) Darriet, J.; Drillon, M.; Villeneuve, G.; Hagenmuller, P. *J. Solid State Chem*. **1976**, *19*, 213.
(19) Zandbergen, H. W.; Ijdo, D. J. W. *Acta Crystallogr*. **1983**, *C39*, 829.

10.1021/cm000277y CCC: $19.00
Published on Web 09/19/2000

alternate with tetrahedral manganese layers. The infrared spectrum of this oxide is consistent with manganese in octahedral and tetrahedral sites corresponding to different oxidation states.

Experimental Section

The system Ba−Ca−Mn−O has been investigated starting from $BaCO_3$, $CaCO_3$, and Mn_2O_3 weighted in stoichiometric $Ba_4Ca_{1-x}Mn_{3+x}O_{12-\delta}$ proportions, with x ranging from 0 to 0.5. The mixtures were ground in an agate mortar and heated in air at 900 °C for 2 days up to a complete decarbonation of the sample. The powders were reground, pressed into bars, and then put in a furnace at 800 °C and heated at 1400 °C for 48 h. The heating and cooling to 800 °C were carried out in 2 h.

Lattice parameters were refined from X-ray powder diffraction data (XRPD) registered with a Philips vertical diffractometer equipped with a secondary graphite monochromator (Cu Kα radiation). Data were collected by step scanning of 0.03° for 4 to 120° and treated by profile analysis with the FULLPROF program (version 3.5-LLB-JRC).[20]

The electron diffraction (ED) study was carried with a JEOL 200 CX microscope, fitted with an eucentric goniometer (±60°), and the high-resolution electron microscopy (HREM), study with a TOPCON 002B microscope (point resolution of 1.8 Å). Both microscopes are equipped with an energy dispersive spectroscopy (EDS) analyzer.

The magnetic measurements as a function of temperature were performed on a Quantum Design SQUID magnetometer and a Faraday balance in a magnetic field of 0.3 T.

Oxygen content was determined from chemical analysis, using redox titration. The infrared (IR) skeletal spectra were recorded with a Nicolet Magna 750 Fourier transform instrument. The skeletal spectra in the region between 400 and 1000 cm^{-1} have been recorded with KBr pressed disks and with a KBr beam splitter.

Results and Discussion

If one scans the $Ba_4Ca_{1-x}Mn_{1+x}O_{12-\delta}$ system, the powder X-ray diffraction patterns allows a new phase to be synthesized. However, a 2L $BaMnO_3$-type minority phase[21] (SG: $P6_3m$; $a = 5.672$ Å; $c = 4.71$ Å) is always observed, whatever x. The actual composition of the new phase does not depends on the nominal x value and remains close to $Ba_4Ca_{0.9}Mn_{3.1}O_{12-\delta}$. Chemical analysis leads to 11.3(1) oxygen per formula unit. All our attempts to obtain a perfectly single-phase sample, by modifying the different parameters of the synthesis process, failed. Adding copper oxide (0.1 mol of CuO/$BaCO_3$) to the starting mixture and heating the bars at 1200 °C for 15 h after decarbonation leads to a prime phase without any visible extra peaks on the XRD pattern. The EDX analyses show that, in the limit of accuracy of the technique, there is no copper in the crystallites. Thus, CuO appears to act as catalyst or doping element, as often observed in the Ba-based hexagonal perovskite.[8,9]

HREM Study: Evidence for a Hexagonal 16L Stacking. The reconstitution of the reciprocal space by tilting around the crystallographic axes showed a hexagonal cell with $a \approx 5.8$ Å, $c \approx 39$ Å, and no conditions limiting the reflection. The compatible space groups are $P6$, $P\bar{6}$, $P6/m$, $P622$, $P6mm$, $P\bar{6}m2$, $P\bar{6}2m$, and $P6/mmm$. The diffraction spots are very sharp without any diffuse streaks along c^*. A typical [1$\bar{2}$0] ED pattern is given in Figure 1a.

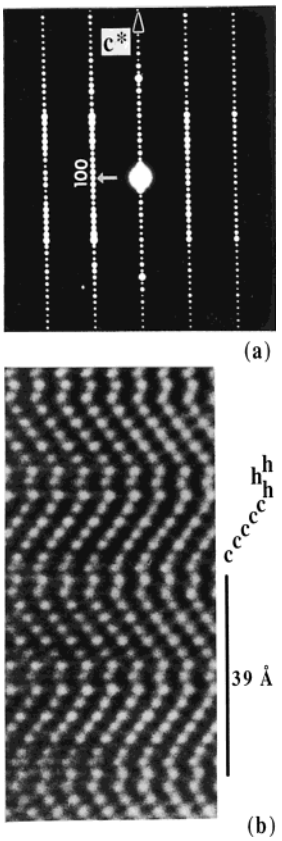

Figure 1. (a) [1$\bar{2}$0] ED pattern of $Ba_4Ca_{0.9}Mn_{3.1}O_{11.3}$ and (b) enlarged [110] HREM image of $Ba_4Ca_{0.9}Mn_{3.1}O_{11.3}$.

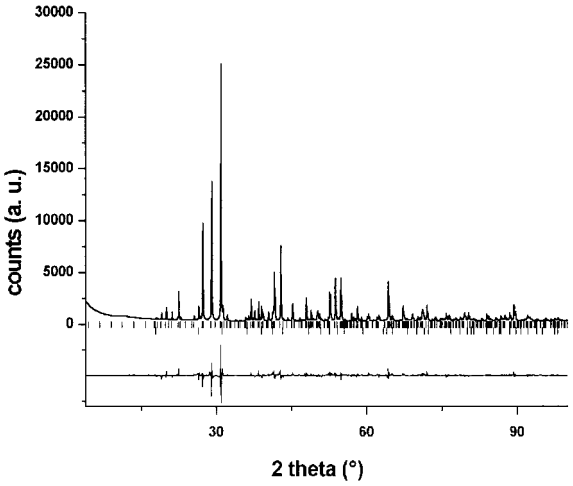

Figure 2. Part of the X-ray powder diffraction and difference patterns ($2\Theta \leq 100°$) issued from refinement of $Ba_4Ca_{0.9}Mn_{3.1}O_{11.3}$. The positions of the Bragg reflections (top, $Ba_4Ca_{0.9}Mn_{3.1}O_{11.3}$; bottom, $BaMnO_3$ 2L) are shown by small vertical lines.

The parameters of the hexagonal $Ba_4Ca_{0.9}Mn_{3.1}O_{11.3}$ cell were refined from XRD data (Figure 2) to $a = 5.8003(3)$ Å and $c = 38.958(1)$ Å.

Considering the c parameter and the usually observed average thickness of the [AO_3] layers in the hexagonal polytypes, a 16L-type structure can be expected. However, several (h, c) stacking modes can be proposed. As reported a long time ago,[22] electron microscopy is a very

(20) Rodriguez-Carjaval, J. *Abstracts of Satellite Meeting on Powder Diffraction of the XVth Congress of the International Union of Crystallography;* Toulouse, France; Oxford University Press: Oxford, U.K., 1990; p 127.

(21) Hardy, A. *Acta Crystallogr.* **1962**, *15*, 179.

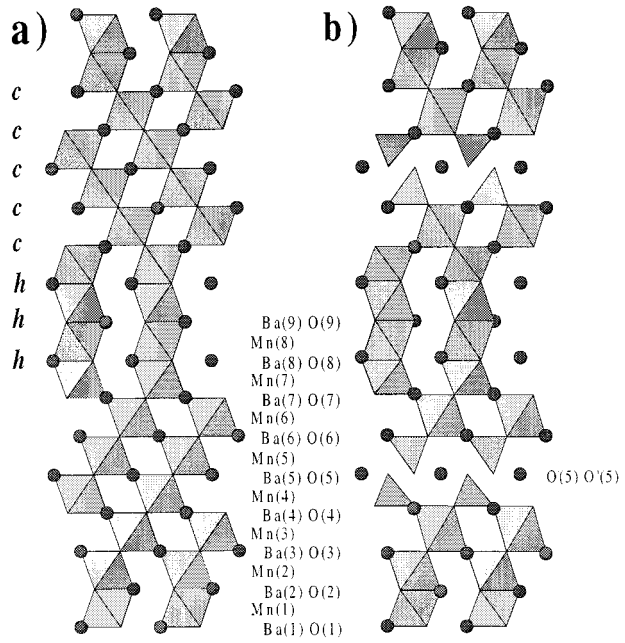

Figure 3. (a) [110] projection of the structural model of the 16L hexagonal perovskite deduced from HREM study and (b) [110] projection of the structural model determined by XRPD.

efficient tool for determining the layer stacking mode along the *c* axis. An example of relevant [110] HREM image is given in Figure 1b. In hexagonal perovskites, the contrast of the [110] images consists of broken lines of dots and the straight segments correspond to adjacent cubic (*c*) close-packed [BaO_3] layers, every change of slope being associated with the presence of hexagonal (*h*) [BaO_3] layers. The focus value is assumed to be close to −55 nm; i.e., the high electron density zones appear as the brighter dots. For eight adjacent bright dots, segments of seven aligned bright dots are associated with three slope changes; then the same sequence is imaged in a mirror up to a 16L periodicity. This contrast is interpreted as an $(hhhccccc)_2$ sequence.

These observations show that $Ba_4Ca_{0.9}Mn_{3.1}O_{11.3}$ either exhibits the hexagonal 16L structure or is closely related to this structural type. Such a structure (Figure 3a) in which blocks of four face-sharing octahedra (hexagonal *h*) alternate with blocks of six corner-sharing octahedra (cubic *c*) seems to be very rare, since we did not find any example of manganese oxides belonging to the 16L type structure.

XRD Structure Refinement: Structural Model. Only the $P\bar{6}$ and $P\bar{6}m2$ space groups are compatible with such an $(hhhccccc)_2$ model. Structural calculations were performed from XRPD data, considering the most symmetric one $P\bar{6}m2$. The small difference between the scattering factors of Ca^{2+} and of Mn^{3+} or Mn^{4+} for X-ray makes the two cations hardly differentiable, so that we considered that they are statistically distributed over the same crystallographic sites. In a first step, we also considered that oxygen vacancies are randomly distributed over the whole oxygen framework. Considering the $P\bar{6}m2$ space group, 26 independent atoms are necessary to describe the model (Figure 3a). To limit the number of variable parameters, some of the positional parameters were constrained. The *z* parameters of Mn(1) to Mn(4), Ba(2) to Ba(4), O(2) to O(4) and of Mn(5) to Mn(8), Ba(6) to Ba(8), and O(6) to O(8) were taken symmetrical with regard to 1/4, respectively; the *x* and *y* values of the oxygen atoms were fixed at ideal values and not refined. Moreover, for each kind of atoms, a same isotropic *B* factor was considered. After refinement of the positional parameters and *B* factors, a $R_{Bragg} = 0.087$ was obtained but the thermal factor of oxygen remained at a too high value ($B_o \approx 3$ Å^2).

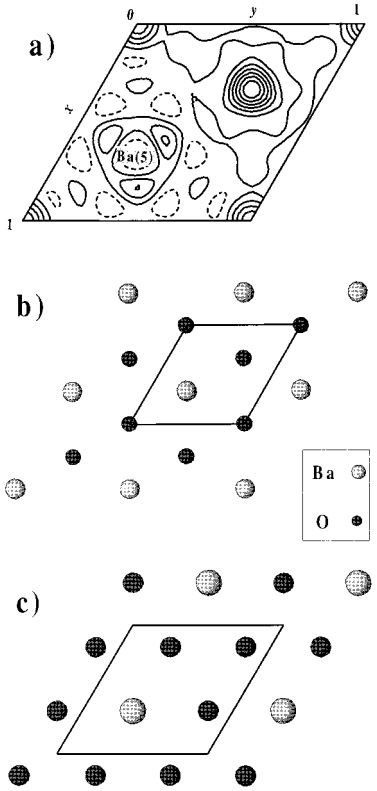

Figure 4. (a) Fourier difference map of $Ba_4Ca_{0.9}Mn_{3.1}O_{11.3}$ at $z = 0.25$, (b) representation of the [BaO_2] layer, and (c) representation of the [BaO_3] layer.

In a second step, the *B* factor and the site occupancy τ of each of the oxygen atoms were separately refined. For the oxygen O(5) in 6*n* with $x = 0.1667$, $y = 0.8333$, and $z = 1/4$, one obtained $B = 42$ Å^2 for $\tau = 1$ and $\tau = 0.3$ for $B = 0.9$ Å^2, suggesting that this site is partially occupied or empty or that its positional parameters are erroneous.

O(5) was then removed, and Fourier difference map sections were calculated. Figure 4a shows that, for $z = 0.25$, two residues are observed at [$x = y = 0$] and [$x = 0.33$; $y = 0.66$] which can be attributed to two new different atomic positions for oxygen labeled O(5) in 2*g*, 0, 0, *z*, and O′(5) in 2*h*, 1/3, 2/3, *z* (with $z \approx 0.25$). With these new oxygen positions, the R_{Bragg} factor is decreased to 0.067 for the variable parameters given in Table 1 ($R_P = 0.097$ and $R_{wp} = 0.128$). This result shows that this hexagonal 16L structure is oxygen deficient at $z = 0.25$, six oxygen atoms (in 6*n*) being replaced by four oxygens atoms (in 2*g* and 2*h*).

The structure of $Ba_4Ca_{1-x}Mn_{3+x}O_{12-\delta}$ (Figure 3b) is directly derived from the hexagonal 16L perovskite (Figure 3a) by replacing MnO_6 octahedra by MnO_4 tetrahedra at the level of cubic close-packed layers ($z \approx 0.25$). At this level, stoichiometric [BaO_3] cubic (*c*) layers

(22) Jacobson, A.; Hutchinson, J. L. *J. Solid State Chem.* **1980**, *35*, 334.

Table 1. Final Refined Structural Parameters for $Ba_4Ca_{0.9}Mn_{3.1}O_{11.3}$

atom	site	*x*	*y*	*z*	*B* (Å^2)
Mn/Ca(1)[a]	2g	0.0	0.0	0.0308(2)	0.14(7)
Mn/Ca(2)[a]	2g	0.0	0.0	0.0959(2)	0.14(7)
Mn/Ca(3)[a]	2i	2/3	1/3	0.1522(2)	0.14(7)
Mn(4)	2h	1/3	2/3	0.2095(2)	0.14(7)
Mn(5)	2g	0	0	0.2905(2)	0.14(7)
Mn/Ca(6)[a]	2i	2/3	1/3	0.3478(2)	0.14(7)
Mn/Ca(7)[a]	2h	1/3	2/3	0.4040(2)	0.14(7)
Mn/Ca(8)[a]	2h	1/3	2/3	0.4692(2)	0.14(7)
Ba(1)	1c	1/3	2/3	0.0	0.74(3)
Ba(2)	2i	2/3	1/3	0.05730(8)	0.74(3)
Ba(3)	2h	1/3	2/3	0.10981(9)	0.74(3)
Ba(4)	2g	0.0	0.0	0.17785(9)	0.74(3)
Ba(5)	2i	2/3	1/3	0.25	0.74(3)
Ba(6)	2h	1/3	2/3	0.32215(9)	0.74(3)
Ba(7)	2g	0.0	0.0	0.39019(9)	0.74(3)
Ba(8)	2i	2/3	1/3	0.44270(8)	0.74(3)
Ba(9)	1b	0.0	0.0	0.5	0.74(3)
O(1)	3j	0.83333[b]	0.16666[b]	0.0	0.8(2)
O(2)	6n	0.16666[b]	0.83333[b]	0.0606(4)	0.8(2)
O(3)	6n	0.83333[b]	0.16666[b]	0.1214(4)	0.8(2)
O(4)	6n	0.50000[b]	0.50000[b]	0.1941(4)	0.8(2)
O(5)	2g	0	0	0.2500[b]	0.8(2)
O(5)	2h	1/3	2/3	0.2500[b]	0.8(2)
O(6)	6n	0.83333[b]	0.16666[b]	0.3060(4)	0.8(2)
O(7)	6n	0.50000[b]	0.50000[b]	0.3786(4)	0.8(2)
O(8)	6n	0.16666[b]	0.83333[b]	0.4394(4)	0.8(2)
O(9)	3k	0.50000[b]	0.50000[b]	0.5	0.8(2)

[a] Mn/Ca = 1.4/0.6. [b] Parameters not refined.

of the 16L structure (Figure 4b) are replaced by ordered oxygen deficient [BaO_2] layers (*c*′) (Figure 4c). Thus, this structure can be described by the stacking along $\vec{c}$ of quadruple layers of face-sharing octahedra (hexagonal *h* layers), with octahedral and tetrahedral layers (belonging to the oxygen deficient cubic *c*′ layers). Such tetrahedral layers have previously been observed in oxygen deficient hexagonal AMO_{3-x} perovskites for M = Fe, Co, and V.[15,22−23]

In the case of manganese, the tetrahedral coordination is not likely for Mn^{3+} or Mn^{4+}, so that higher oxidation state Mn^{6+}/Mn^{7+} should be considered for Mn(4) and Mn(5). The interatomic distances (Table 2), ranging from 1.58 to 1.78 Å, close to those observed in $K_3Mn_2O_8$,[24] for Mn^{7+} (1.60 Å) and Mn^{6+} (1.65 Å) strongly support this viewpoint. The dissolution of this oxide in a mix of phosphoric and hydrochloric acids, leading to the pink coloration characteristic of the presence of manganates or permanganates ions, is the final proof of the Mn^{6+}/Mn^{7+} oxidation state for manganese in tetrahedral coordination.

The ideal composition $Ba_4Ca_{0.9}Mn_{3.1}O_{11.5}$, deduced from the structural refinements, is in perfect agreement with the chemical composition $Ba_4Ca_{0.9}Mn_{3.1}O_{11.3}$, deduced from the redox titration, suggesting the existence of additional oxygen vacancies within the octahedral layers but with a too weak concentration to be detected by XRPD data. Bearing in mind the presence of Mn^{6+}/Mn^{7+} species on tetrahedral sites, this implies that the octahedral sites are occupied by calcium and Mn^{3+} or eventually by Mn^{4+} and Mn^{2+} species. Concerning the distribution of calcium in octahedral sites, it is worth pointing out that the significantly larger Mn−O distances observed for Mn(3) and Mn(6) suggest that those

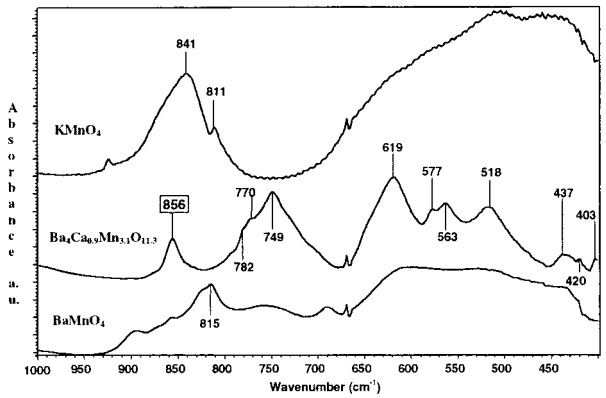

Figure 5. IR spectra for $BaMnO_4$, $KMnO_4$, and $Ba_4Ca_{0.9}Mn_{3.1}O_{11.3}$.

Table 2. Interatomic Distances

M−O	×*n*	*d* (Å)	M−O	×*n*	*d* (Å)
Mn/Ca(1)−O(1)	×3	2.060(5)	Ba(2)−O(2)	×6	2.903(1)
−O(2)	×3	2.04(1)	−O(3)	×3	3.01(1)
Mn/Ca(2)−O(2)	×3	2.17(1)	Ba(3)−O(2)	×3	2.55(1)
−O(3)	×3	1.95(1)	−O(3)	×6	2.935(3)
Mn/Ca(3)−O(3)	×3	2.06(1)	Ba(4)−O(3)	×3	2.762(1)
−O(4)	×3	2.34(1)	−O(4)	×6	2.968(3)
			−O(5)	×1	2.811(3)
Mn(4)−O(4)	×3	1.78(1)			
−O′(5)		1.58(1)	Ba(5)−O(4)	×3	2.75(1)
			−O(5)	×3	3.35(1)
Mn(5)−O(5)		1.58(1)	−O(5)	×3	3.35(1)
−O(6)	×3	1.78(1)	−O(6)	×3	2.75(1)
Mn/Ca(6)−O(6)	×3	2.34(1)	Ba(6)−O′(5)	×1	2.811(3)
−O(7)	×3	2.06(1)	−O(6)	×6	2.968(3)
			−O(7)	×3	2.762(1)
Mn/Ca(7)−O(7)	×3	1.95(1)			
−O(8)	×3	2.17(1)	Ba(7)−O(7)	×6	2.935(3)
			−O(8)	×3	2.55(1)
Mn/Ca(8)−O(8)	×3	2.04(1)			
−O(9)	×3	2.060(5)	Ba(8)−O(7)	×3	3.01(1)
			−O(8)	×6	2.903(1)
Ba(1)−O(1)	×6	2.90(1)	−O(9)	×3	2.790(2)
−O(2)	×6	2.89(1)			
			Ba(9)−O(8)	×6	2.89(1)
Ba(2)−O(1)	×3	2.790(3)	−O(9)	×6	2.90(1)

sites are preferentially if not fully occupied by calcium. Nevertheless the distribution of calcium and manganese over the octahedral sites (Mn(1)−Mn(2)−Mn(3)−Mn(6)-Mn(7)−Mn(8)) cannot be further discussed here and will require a neutron diffraction study.

Infrared Spectroscopy. An infrared study of $Ba_4Ca_{0.9}Mn_{3.1}O_{11.3}$ was carried out in order to detect the possible presence of Mn^{6+}/Mn^{7+}−O absorption peaks in tetrahedral coordination. For comparison, the $BaMnO_4$ and $KMnO_4$ spectra were also recorded (Figure 5).

The spectrum of the title compound exhibits, in the region 400−1000 cm^{-1}, several absorption bands whose attribution is very complex due to the presence of manganese and calcium with similar environments.

Considering the reference compounds, $BaMnO_4$ and $KMnO_4$, it can be emphasized that these oxides both exhibit absorptions at 815 and 841 cm^{-1}, characteristic of MnO_4^{2-} and MnO_4^- species, in agreement with what was previously reported: 830 cm^{-1} for the stretching mode of the MnO_4^{2-} ion.[25] In contrast, manganites with the perovskite structure containing Mn^{3+} or Mn^{4+}

(23) Liu, G.; Greedan, J. E. *J. Solid State Chem.* **1994**, *108*, 371.
(24) Hursthouse, M. B. *J. Chem. Soc., Faraday Trans.* **1992**, *88*, 3071.
(25) Brunold, T.; Hazenkamp, M. F.; Güdel, H. U. *J. Am. Chem. Soc.* **1995**, *117*, 5598.

species in octahedral coordination do not show such bands but absorption bands in the region 350−700 cm^{-1}.[26,27]

Despite the great complexity of the structure of the oxide $Ba_4Ca_{0.9}Mn_{3.1}O_{11.3}$, we can assign without ambiguity its absorption band at 856 cm^{-1} to the stretching mode of MnO_4^{2-} or MnO_4^{-} tetrahedra, whereas Mn^{3+} (or Mn^{2+}, Mn^{4+}) should be responsible for the appearance of bands between 400 and 700 cm^{-1}.

Magnetic Properties. Magnetic susceptibility measurements do not show any sign of magnetic ordering down to 10 K. Above 320 K, the thermal variation of the magnetic molar susceptibility obeys the Curie−Weiss law ($\chi = C/(T - \Theta_P)$) (Figure 6) with a $\Theta_P \approx -288$ K and a Curie constant value of 5.63. The corresponding value of the effective moment is 6.7 μ_B per formula unit. Taking into account the complexity of the structural model and the negative value of Θ_P, which supports strong antiferromagnetic interactions, the assignment of manganese oxidation states from these measurements would be risky. Their determination will require the use of other techniques such as XANES.

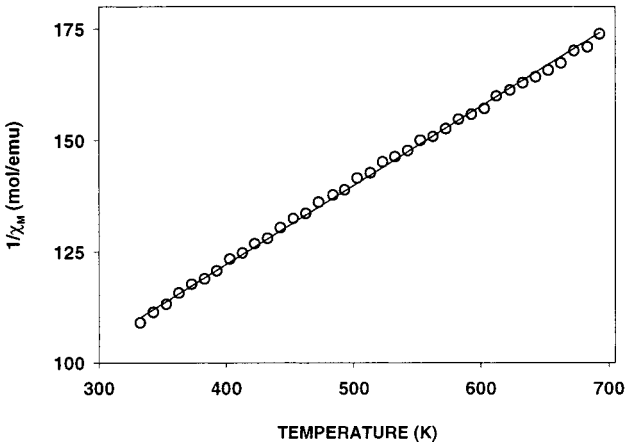

Figure 6. Temperature dependence of χ_M^{-1} in the range 320−700 K for $Ba_4Ca_{0.9}Mn_{3.1}O_{11.3}$ (open circles, experimental points; solid line, Curie−Weiss fit).

Concluding Remarks

In conclusion, a new manganese oxide with an original structure derived from the hexagonal perovskites has been synthesized. Such a hexagonal 16L structure involving tetrahedral layers has never been observed previously and is remarkable since it implies a disproportionation of manganese. A neutron diffraction study will be carried out to determine the exact distribution of the cations in the structure and to obtain a better accuracy on the oxygen positions. These results open the route to the research of other manganese oxides characterized by a Mn disproportionation.

Acknowledgment. The authors are grateful to Dr. N. Nguyen for magnetic susceptibility measurements and to Pr. M. Daturi for his help in the infrared study.

CM000277Y

(26) Rao, G. V.; Rao, C. N. R. *App. Spectrosc.* **1970**, *24*, 436.
(27) Roy, C.; Rao, R. C. *J. App. Phys.* **1999**, *85*, 3124.